

Tectonophysical Features of the Load–Unload Response Ratio (LURR) Caused by the Tokachi-Oki Earthquake (September 25, 2003, $M_w = 8.3$)

A. S. Zakupin^a, * and A. Yu. Polets^a

^a Institute of Marine Geology and Geophysics, Far East Branch, Russian Academy of Sciences, Yuzhno-Sakhalinsk, 693022 Russia

*e-mail: a.zakupin@imgg.ru

Received July 21, 2023; revised February 4, 2024; accepted March 14, 2024

Abstract—The paper presents the results of retrospective and tectonophysical analysis of the Tokachi-Oki earthquake source area on the September 25, 2003 ($M_w = 8.3$). Particular attention is paid to the Hidaka tectonic belt, the structures of which were affected by the Tokachi-Oki earthquake. The load–unload response ratio (LURR) method was applied at sufficient spatial (a square with a side of about 400 km) and temporal (continuous 20-year period) intervals to consider the results reliable. The forerunners of the Tokachi-Oki earthquake on the September 25, 2003, were revealed (on average, two years before the seismic event), which strictly determined the earthquake location. The data obtained with The method of cataclastic analysis (MCA), together with LURR data, made it possible to establish the stages of instability development in the Hidaka collision zone. The Hidaka tectonic belt became outlined by destruction zones (mainly horizontal compression) from 1997 to 2003 (up to the Tokachi-Oki earthquake). LURR anomalies were detected along the belt a couple of years before the earthquake. The prediction of the Tokachi-Oki earthquake by the LURR method is one of the most reliable in our practice.

Keywords: earthquakes, earthquake prediction, stress state, Hidaka zone

DOI: 10.1134/S1819714024700118

INTRODUCTION

On September 25, 2003, at 19:50 UTC, an earthquake with a moment magnitude $M_w = 8.3$ occurred near Hokkaido, Japan [55]. The earthquake caused extensive damage and landslides. The height of tsunami waves reached 4 m [27]. The event was subsequently called the Tokachi-Oki earthquake.

Like any event of this magnitude, the Tokachi-Oki earthquake is mentioned in many studies on forecasting earthquakes, either directly or indirectly. In [34, 45], this earthquake was predicted 6 months before its manifestation. The Reverse Tracing of Precursors (RTP) method was used for forecasting. The authors of [34, 45] suggest that the forerunner is a dense sequence of small earthquakes that rapidly propagate over long distances. According to their opinion, a strong earthquake is expected within 9 months after the formation of such a sequence within a formally defined setting.

Microseismic vibrations within periods of a few minutes recorded before the Tokachi-Oki earthquake were analyzed in [47]. A series of asymmetric pulses occurring several days before the earthquakes was revealed. In [54], an ionospheric anomaly was

detected based on variations in the total electron content derived from GPS measurements. The anomaly was detected several days before the main event near the epicenter. According to data obtained from microbarographs [48], a change in atmospheric pressure before the Tokachi-Oki earthquake was recorded. The pressure change began with the arrival of a body wave and reached the maximum amplitude with the arrival of a surface Rayleigh wave, which allowed the authors of [48] to suggest that the observed change was caused by ground motion produced by seismic waves.

According to [38], strong “shallow” earthquakes along subduction zones sometimes precede the occurrence of strong deep-focus earthquakes. The Tokachi-Oki earthquake (2003) was preceded by noticeable deep seismicity in the subduction slab, including a ($M_w = 6.8$) deep-focus earthquake. According to [39], a change in the temporal parameter of the fractal dimension (D) can be considered another precursor. This study revealed that parameter D began to decrease in 1998 and became very small approximately 1 year before the main shock. Moreover, the decrease in the D value before the main shock is characteristic of some large earthquakes. Hence it follows that this decrease may be an earthquake precursor.

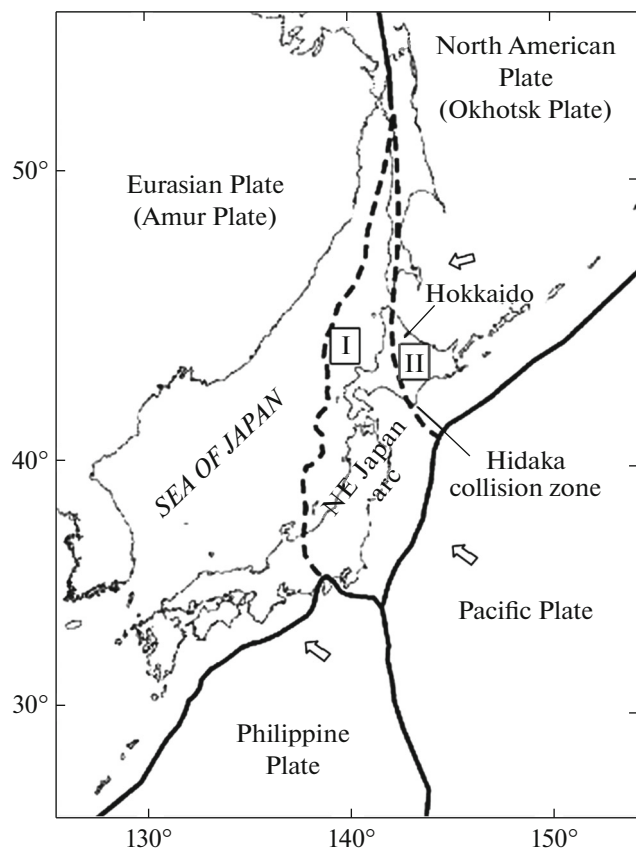


Fig. 1. Possible boundaries of lithospheric plates in north-eastern Japan. I, boundary proposed by Nakamura [40] and Kobayashi [36]; II, boundary proposed in (Chapman and Solomon [30], (from [33])).

In general, a review of previous studies shows that number of signs of preparation of the 2003 earthquake occurred according to various observations and models. Verification of the LURR method in a retrospective analysis of seismic data on the 2003 Tokachi-Oki earthquake could well complement earlier results. To bolster the tectonophysical component of the study, we propose to evaluate the dynamics of the stress-strain state of the medium at all evolutionary stages of the earthquake source (the emergence and development of the anomalous state of the medium according to the LURR method) using the method of cataclastic analysis (MCA) [20].

STRUCTURAL FEATURES OF HOKKAIDO AND THE NATURE OF THE HIDAKA TECTONIC BELT

Hokkaido is located in the active transition zone between the Eurasian continent and the Pacific Ocean, in the geodynamic junction zone of three lithospheric plates: the Pacific, Eurasian (Amur), and Okhotsk (Fig. 1). Such a location of the island governs its tectonic, seismic, and volcanic activity.

It should be noted that the current state of the problem of the boundary between the Eurasian and North American plates is very controversial [25]. In some studies, the Amur and Okhotsk microplates are distinguished at the junction of these plates [24], while in others, they are not [32, 44]. As well, the North American Plate is shown in different ways. According to Ismail-Zadeh et al. [32], the Okhotsk plate is a part of the North American Plate. Its western boundary runs entirely along the axial part of the Tatar Strait, and its southern part covers half of Hokkaido. According to [2], the Japan–Korean block is distinguished between the Amur and Okhotsk microplates. This block should border the Okhotsk block in the east and the Amur Plate in the west. The diffuse boundary between the Eurasian and North American plates is drawn arbitrarily, and there is still no strict substantiation of the position of this boundary.

Within northern Japan, the issue of the position of the boundary between the Eurasian (Amur) and North American (Okhotsk) plates is also ambiguous. In [30], the authors considered the position of the boundary between plates along the central part of Hokkaido (Fig. 1, I). However, in the early 1980s, Nakamura [40] and Kobayashi [36] suggested that the plate boundary shifted to the eastern Sea of Japan (Fig. 1, II) 1–2 Ma [40] or 0.5 Ma [43] ago.

The convergence of adjacent lithospheric plates occurs over a wide range of diffuse zone. One of the important characteristics of the collisional process is the collision deformation rate, i.e., the lateral contraction rate of Earth's crust in the collision zone. Its maximum value cannot exceed the tangential component of the oceanic plate velocity; the actual value shows what part of the total relative motion is transferred to the convergence of island arcs and their deformation in the collision zone [10]. The studies [33] showed that the crustal contraction rate in the central part of Hokkaido has been relatively constant since the Pliocene. As well, about 50% convergence at the relative motion of the plates still occur in the central part of Hokkaido (Hidaka collision zone) and the position of the plate boundary in Northern Japan cannot be marked by a single line.

The present-day structure of Hokkaido was formed in the Middle Miocene due to the oblique collision of the Eurasian and North American plates, accompanied by NS-trending shear and EW-trending thrust movements. As evidenced by the location of active faults and ore veins, these movements continued in the Quaternary and are still ongoing [3].

The Hidaka and East Sakhalin terranes were moved considerable distances not only in meridional direction but also westward along thrust planes during the Cenozoic. This is explained by the location of Island of Hokkaido at the junction of right-lateral Sakhalin thrusts and the same thrusts of the Kuril Islands formed due to oblique subduction of the

Pacific plate as it moved in the sublatitudinal direction. The interaction of the above right-lateral shear systems led to the formation of the Hidaka collision zone in the Late Miocene [35]. As a result, the crust up to 39 km thick (Hidaka zone) was formed [28]. Right-lateral shear displacements on Sakhalin and the Kuril Islands in combination with complex movements of the Oshima terrane caused by the opening of the Sea of Japan, were obviously transformed in Central and Eastern Hokkaido into thrusts of submeridional strike.

According to the geological features, Island of Hokkaido can be divided into three parts: Western (Japanese (Tohoku-Honshu) island-arc system), Central (Hokkaido–Sakhalin folded uplift, arc–arc collision zone), and Eastern (Kuril–Kamchatka island-arc system). All major block systems of Hokkaido are oriented across the strike of the trench and a seismic focal zone. This is rarely observed in island-arc settings. The Kamchatka, Kronotsky, and Shipunsky peninsulas in Kamchatka, near which earthquakes are concentrated, can be considered an analog of such relationships. In a less distinct form, the same is observed in Hokkaido.

The Hidaka–Central Hokkaido Zone is characterized by the most complex geological structure. This zone does not belong to the Japanese or Kuril island arcs in terms of geological structure and covers the area from the eastern border of the Ishikari lowland to the Abashiri tectonic line, crossing the Hidaka Mountains. The formations of the Hidaka zone, which are characterized by western vergence of folded and fault dislocations, are thrust over rock complexes of the eastern part of the pre-Neogene Japan volcanic arc. Structurally, the Hidaka Belt represents a thick right-lateral thrust zone developed along a series of regional faults that caused multiple twinning of sections even before their faulting.

SEISMICITY OF HOKKAIDO

The high seismicity of the Hokkaido block is manifested as a large-number of shallow earthquakes in the upper layers of the seismic focal zone. The main zone of strong earthquakes is confined to the subduction zone of the Pacific oceanic plate beneath the Okhotsk Plate. Earthquake epicenters are located on the ocean floor between the deep-sea trench and eastern banks of Hokkaido. Earthquakes with epicenters located on the island itself and in the Sea of Japan are relatively rare. The seismicity of Hokkaido is heterogeneous even along the subduction zone. Two zones can be distinguished: the Nemuro (the continuation of the Kuril–Kamchatka island arc) and the Hidaka, taking into account its continuation under the ocean floor [1].

A higher seismicity, thrust movements parallel to the trench, and sinistral strike-slip faults observed in

the Hidaka collision zone, are associated with uplift at the frontal edge of the Kuril arc. Based on the distribution of earthquake hypocenters along Hokkaido, the angle of inclination of the upper boundary of the seismic focal zone varies from 20° to 30° from the Japan arc and further to 40° and 50° to the north along the Kuril arc (143°–144° E). The significant curvature of the surface of the seismic focal zone due to the conjunction of the two arcs may be related to extension or rupture of the subducting plate with depth [12].

The block structures transverse to the seismic focal zone affect the distribution of earthquake sources. This is particularly clear with the example of the Kitami–Hidaka horst-anticlinorium. Catastrophic earthquakes with epicenters in the ocean near the Hokkaido coast are associated with the latter. These are the shallow earthquakes of January 4, 1912 ($M = 8.0$), March 4, 1952 ($M = 8.3$), and March 21, 1982 ($M = 7.2$).

The Tokachi-Oki earthquake on September 2003, $M_w = 8.3$ continued the succession of strong earthquakes associated with the Hidaka zone and its seismic activity. The earthquake on September 25, 2003 was accompanied by a large series of aftershocks. The source parameters obtained from *P*- and *S*-wave analysis data are as follows: seismic moment 1.0×10^{21} H m, stress release 50 TPa, onset of rupture at depth of 25 km, rupture duration 40 s, maximum displacement 5.8 m, average displacement 2.6 m, rupture area 90×70 km² [49]. According to bottom seismographs, a seafloor uplift of 37 ± 5 cm was recorded directly in the hypocentral zone [46].

It should be noted that the same section of the fault was ruptured as during the earthquake with $M = 8.3$ in 1952. An earthquake source was located on the shelf near Cape Erimo and had a length of 100 km. The shaking intensity was 8 MSK. Earthquakes on March 4, 1952, and September 25, 2003, are associated with megathrusts, which occurred as a result of segmental rupture of the Pacific Plate beneath the Hokkaido–Tohoku accretionary wedge [41]. The source area of the Tokachi-Oki earthquake is $\sim 1.4 \times 10^4$ km² and partially coincides with the seafloor deformation area ($\sim 2.52 \times 10^4$ km²) associated with the 1952 earthquake [49].

There was NE-trending subvertical overthrusting (with left-lateral shear components) or an ENE-trending thrusting (with right-lateral shear components).

The motion in the main shock source on September 25, 2003, occurred predominantly under the action of SE-trending compression stresses. The type of motion in the source is NE-trending low-angle thrusting (with right-lateral shear components). According to geological and tectonic data, the earthquake source (September 25, 2003) was located southeast of the Erimo Peninsula on the continental slope in the transform zone of the Hidaka submarine uplift, at

the boundary between the Japan and Kuril–Kamchatka segments of the deep-water trough [9]. The rupture line of the Tokachi–Oki earthquake is localized at the boundary between the highly anisotropic setting (the Hidaka Mountains) and the low-anisotropic setting (the Tokachi Plain).

INITIAL DATA

For calculations, we used data on earthquakes (including focal mechanism solutions for the MCA) of the NIED Catalog (National Research Institute for Earth Science and Disaster) [56]. For calculation using the LURR method, we chose samples of earthquakes from this catalog with magnitudes from 3.3 to 5.0 in nine circular areas. An average number of earthquakes in each working sample was about 1000 earthquakes for the 20-year calculation period. Also, a working catalog was created based on the NIED catalog data for the study region following the MCA. The catalog included 362 events with a magnitude range of $3.1 \leq M_w \leq 6.9$ over a period from January 1, 1997 to September 25, 2003. The depth interval for reconstruction was 0–30 km (the depth of the GCMT centroid forming the earthquake on September 25, 2003, $h = 28.2$ km). No depth limitation was applied for LURR calculations. The most representative magnitude ranges are from 3.1 to 3.9 (178 events) and from 4.1 to 4.9 (153 events). Earthquake mechanisms in the magnitude range of $3.1 \leq M_w \leq 5.9$ were identified for reconstruction. As well, four events with $M_w \geq 6.0$ were excluded. The use of a difference of more than 2.5–3 units in the magnitude ranges leads to overestimation of the role of strong earthquakes, since the mechanisms of these strong events begin to participate in determining the stresses of most domains, significantly averaging the results of calculations [22].

We analyzed the working catalog by kinematic type of focal mechanisms before the Tokachi–Oki earthquake on September 25, 2003 (362 events) and in the aftershock period (324 events). The classification was proposed by M.I. Streltsov [16] based on the angles of inclination to the horizon of nodal planes (DP1, DP2) and angle (PI) of the N axis: from January 1, 1997 to September 25, 2003: reverse faults, 253 events (70, *the percentage of the number of earthquakes in this group*); thrust faults, 21 events (6); normal faults, 67 events (21); oblique faults, 4 events (1); strike-slip faults, 21 events (6). In the period from September 26, 2003 to September 26, 2004: reverse faults, 198 events (61); thrust faults, 11 events (3); normal faults, 67 events (21); oblique faults, 6 events (2); strike-slip faults, 42 events (13). The focal mechanisms of the strongest earthquakes (12 events) $M_w \geq 6.0$ (not participating in the reconstruction) are reverse and thrust faults.

The processing of initial seismic data was performed in long-period (January 1, 1997–September 25, 2003) and short-period (1997–1999; 2000–2001;

2002–2003; 2003–2004) regimes of reconstruction using the MCA in $0.1^\circ \times 0.1^\circ$ grid nodes in the lateral direction. The procedures of forming uniform samples of earthquake focal mechanisms were performed for 188 (1997–1999); 73 (2000–2001); 101 (2002–2003) 439 (1997–2003); and 267 (2003–2004) quasi-homogeneous domains. The average stress tensor parameters for the entire observation period were calculated for each of the domains.

In total, 12 earthquakes with $M_w \geq 6.0$ occurred in the studied region over the considered time interval: February 20, 1997 ($M_w = 6.0$, $h = 47$ km), October 8, 1997 ($M_w = 6.0$, $h = 8$ km), November 15, 1997 ($M_w = 6.0$, $h = 157$ km), May 30, 1998 ($M_w = 6.1$, $h = 15$ km), May 12, 1999 ($M_w = 6.2$, $h = 96.2$ km), October 3, 2000 ($M_w = 6.2$, $h = 15$ km), August 13, 2001 ($M_w = 6.4$, $h = 44$ km), December 2, 2001 ($M_w = 6.4$, $h = 123.7$ km), October 14, 2002 ($M_w = 6.1$, $h = 48$ km), November 3, 2002 ($M_w = 6.4$, $h = 44$ km), May 26, 2003 ($M_w = 7.0$, $h = 61$ km), July 25, 2003 ($M_w = 6.0$, $h = 15$ km).

RESEARCH METHODS

The LURR method was developed by Chinese seismologists in the 1990s [51]. When justifying the method, it was assumed that the prediction sign of approaching failure of a continuum in the earthquake focal zone is an increase in some parameter characterizing the difference between the load curve $\sigma = f(\epsilon)$ of Hooke's law. The authors of [50] imply that the load curve for the principal stress and strain (one of the components of these tensor values) can describe the behavior of the material of the medium in a region that is much larger than the preparing source, under the influence of lunisolar tides.

Independently of the Chinese seismologists, A.V. Nikolaev [14, 15] also considered the relationship between earthquakes and the phases of tidal disturbances. Despite insignificant differences in the statistical analysis method, both Chinese and Russian studies yielded similar results. In case of the LURR method, attention was paid to the difference of deformation responses of the medium at different tidal phases. A necessary condition for the appearance of such a difference is the nonlinearity of the dependence $\sigma(\epsilon)$, the appearance of which is associated with the process of damage accumulation:

$$\sigma(\epsilon) = E_0[1 - D(\epsilon)]\epsilon, \quad (1)$$

where σ is the the principal principal stress stress; ϵ is the corresponding elastic component; E_0 is the elastic modulus; D is the measure of material damage introduced according to [37]. The parameter D increases with increasing ϵ from 0 to 1. In some studies, e.g., [13], the time dependence of parameter D is linked to the concentration of microcracks. The inelasticity of the medium determines the difference of deformation

variations $\delta\varepsilon_+$, $\delta\varepsilon_-$ (plus and minus indicate the direction of the tidal gradient). If the stress increases and decreases by the same magnitude $\delta\sigma$, the absolute magnitudes of all variations are considered. The ratio of strain responses to load and unloading R_ε can serve as a quantitative characterization of the inelasticity of deformation at this stage of process:

$$R_\varepsilon = \frac{\delta\varepsilon_+/\delta\sigma}{\delta\varepsilon_-/\delta\sigma} = \frac{\delta\varepsilon_+}{\delta\varepsilon_-}, \quad (2)$$

The R_ε ratio can be expressed in terms of the values entering into expression (1) using the following formula (intermediate calculations are omitted):

$$R_\varepsilon = 1 + \frac{2\sigma}{E_0(1-D)} \frac{dD/d\varepsilon}{d\sigma/d\varepsilon}. \quad (3)$$

In the lack of accumulation of defects with increasing strain (or stress), the derivative $dD/d\varepsilon = 0$ and $R_\varepsilon = 1$. Expression (3) shows that the R_ε values can differ significantly from unity only at the plastic deformation site, when the slope of the tangent to the strain curve decreases significantly. In addition, the strain itself $\varepsilon = \sigma/[E_0(1-D)]$ is finite. In terms of recent work [11], this condition can be rephrased as a decrease in the effective stiffness of the host medium. At the point of transition to the superlimiting deformation, where $d\sigma/d\varepsilon = 0$, the expression for R_ε loses correctness, but the failure in the medium (earthquake) occurs already at the superlimiting section of deformation. This pre-determines that the strain response R_ε (a sign of increasing plastic deformation) can be informative as a mid-term precursor (weeks-months), but not as a short-term precursor of a strong earthquake (hours-days).

It was proposed in [50, 51] to consider the LURR parameter Y_m instead of the strain response ratio R_ε . This parameter is the ratio of responses of a sequence of seismic events to test loading and unloading. Lunisolar tides were chosen as test stress changes. The LURR parameter was introduced for additive quantities: seismic energy, Benioff strain and seismic event accumulation using the relation

$$Y_m = \sum_{i=1}^{N^+} (E_i^m)_+ / \sum_{i=1}^{N^-} (E_i^m)_-. \quad (4)$$

In expression (4), E_i denotes the seismic energy of event numbered i , which can be calculated by energy class ($E = 10^K$, [17]). The latter, in turn, is related to magnitude ($K = 1.8M + 4$). The “+” sign indicates events that occurred during the load increment period; the “-” sign indicates events during unloading. The degree index m takes the values $m = 1, 1/2, 0$. When $m = 1$, the parameter $Y_1 = Y_E$ represents the ratio of the released seismic energy during the periods of stress increase and decrease, respectively, due to tides. At $m = 1/2$, this parameter describes the ratio of the Benioff strain response at the same tidal phases, $Y_{1/2} = Y_B$.

When $m = 0$, it reduces to the ratio of the number of N_+ , N_- , events that occurred during loading and unloading, respectively ($Y_0 = Y_N = N_+ = N_-$). Tidal perturbations are considered positive at the phase of the tide when the shear stress acting along the surface increases. According to the Coulomb–Mohr law, slip-page along this surface occurs the most easily [31]. It should be noted that, when constructing the ratio of the number of N_+/N_- events in the periods of load and unloading growth [14, 15], these periods were chosen somewhat differently: by perturbations of the vertical stress component (the addition to the lithostatic pressure corresponds to the positive phase).

To process the data using the LURR method, the Seis-ASZ software package, developed at the Institute of Geology and Geophysics, Far Eastern Branch, Russian Academy of Sciences was used [4]. To perform calculations, we have developed methods that are universal in the choice of processing parameters and make it possible to replicate the results [6]. In contrast to earlier studies by our colleagues (see, e.g., review [53]), in which the evaluation parameters are changed for each forecast, this approach makes cannot be used for operational forecasting. In our studies, these parameters have fixed values: the magnitude range in the working sample is 3.3–5.0, the moving window is 360 days, and the computational domain is a circle with a radius of 1° . Using the above parameters in LURR calculations, we performed successful retrospective earthquake forecasting for different parts of Sakhalin Island [5–8].

At the first stage of the calculation, the components of tidal displacements formed due to the gravitational potential during the interaction of the three-body system Earth–Sun–Moon are calculated for the epicenter of each earthquake. Tidal calculations are performed in accordance with the algorithm implemented in Berger’s ERTID software [29]. The stress tensor components are calculated based on a rigid and elastic Earth model (with three elastic constants). The stresses are calculated at several points before, during, and after the earthquake so as to determine the dynamics of the tidal component. The resulting stresses are used to calculate the Mohr–Coulomb failure criterion and to determine the dynamics of the effective shear stress. As a result, a role, which tidal disturbances played at the time of failure (or movement), is determined for each earthquake, whether they decreased or increased the effective shear stress. The first-type earthquakes become conditionally “negative” and the second-type earthquakes—“positive”. The equations of continuum mechanics for the above calculations are fully consistent with those used by the authors of the method [52], but this calculation has a series of restrictions. In particular, the peculiarities of the earthquake focal mechanism and the influence of the ocean tide are not fully taken into account [23].

At the final step, the LURR parameter (Eq. 4) is calculated. Different researchers may come to variant results at this stage, as they depend on the choice of parameters of the computational model, including the base parameter for Eq. 4 (we use the Benioff deformation; in Eq. 4 the parameter $m = 0.5$). The size of the summation window is 360 days. The window is moved in 30-day increments over the calculation period. It is important to remember that the point on the graph corresponds to the middle of the averaging window, i.e., the actual data are used in the calculation six months ahead. The discrimination level (threshold for anomaly detection) in the LURR parameter distribution plots is set to 3. Exceedances of the threshold of impulse character (exceedance in one point at a step of 30 days) are not considered anomalies. We accepted such a condition when processing on the basis of the previously analyzed statistics. Most of such outbursts were not relevant to the forecasting issues. In [8], the alarm period (the time interval after the appearance of an anomaly, the period when an earthquake should be expected) is defined. A 3-year period was chosen as the maximum alarm period.

To study the stress state before and after the Tokachi-Oki earthquake (September 25(26), 2003), the MCA was used [18–23, 42].

The main MCA algorithms are presented in monograph [20]. An important feature of the method is the selection of quasi-uniformly deformable domains, within which a uniform sample of earthquake focal mechanisms is formed. The MCA algorithm includes procedures for selecting such earthquakes based on the energy principles of plasticity theory (elastic strain energy dissipation at fault displacements).

The selected sets of earthquakes satisfying the condition of positive dissipation of elastic energy are called homogeneous earthquake samples. They are used to determine the parameters of the ellipsoid of stress tensors and seismotectonic deformation increments (principal stresses and type of ellipsoid) normalized to the value of the shear intensity, and to characterize the quasi-homogeneously deformed section of the Earth's crust (domain) to which the results of stress calculation are attributed.

The stress–strain state parameters are calculated in the lateral direction in grid nodes. Based on the spatial proximity criterion, the earthquakes with elastic unloading domains, which have a mutually intersecting zone including the calculation node, are selected. The earthquake sample created on the basis of this criterion is called the initial sample of earthquake focal mechanisms. Further, the creation of uniform samples is carried out by successive time scale-based searching of events from the initial sample. The uniform sampling with a sufficient number of events is followed by the calculation of parameters of stress tensors and seismotectonic strain increments. Several uniform samples of earthquake focal mechanisms can correspond

to each calculation node. This approach allows us to distinguish several phases of quasi-homogeneous deformation for a single microvolume.

When determining the orientation of the principal stress axes of the stress tensor and the Lode-Nadai coefficient value, we select such a stress state from all possible ones, for which the set of earthquake focal mechanisms being analyzed provides the maximum dissipation of energy accumulated in elastic deformations [20].

In recent years, major advances have been noted in studying natural stress state (shear fractures or earthquake focal mechanisms) of seismically active regions on the basis of MCA [19–21]. Thus, this method is applicable both for estimating the parameters of the present-day stress state from data on earthquake focal mechanisms and for reconstructing paleostresses based on the slip planes in natural outcrops [42].

One of the directions of application of tectonic stress parameter data is also seismic zoning of the territory, according to which it is possible to divide the fault zones by degree of their preparation for the realization of large earthquakes. At the same time, the zoning pattern changes, requiring ongoing monitoring of the tectonic situation. The detail of zoning is determined by a scale level of the reconstructed stress field and by the most representative magnitude range of the catalog of focal mechanisms used for reconstruction [20].

RESULTS

The LURR analysis was conducted in the scanning mode over an area sufficient to cover the activation volume corresponding to the level of the studied earthquake. For this, the earthquake epicenter was surrounded by nine calculation circular domains within the zone with coordinates: 40° N–44° N, 142° E–146° E (map in Fig. 2a). The centers of the circular domains were placed at one-degree intervals in latitude and longitude. The calculation circular domains with a one-degree radius were placed arbitrarily regardless of the Tokachi-Oki earthquake epicenter. In addition, for comparison (the scan mode off), calculation was also performed in a circular domain centered at the epicenter. Over a 20-year period, 1170 earthquakes with $M_w = 3.3–5.0$ (the working sample for calculating the LURR parameter) were recorded. Figure 2b shows the graph of LURR variation from 2000 to 2020 in the calculation domain centered at the earthquake epicenter. One anomaly per 20 years is observed in the calculation circular domain. Exceeding the threshold equal to three (the divisions on the graph correspond to the middle of the smoothing window) occurred 21 months before the Tokachi-Oki earthquake (December 2001).

Let us consider the results in nine arbitrary regions. Figures 3a–3i show the plots of the LURR parameter

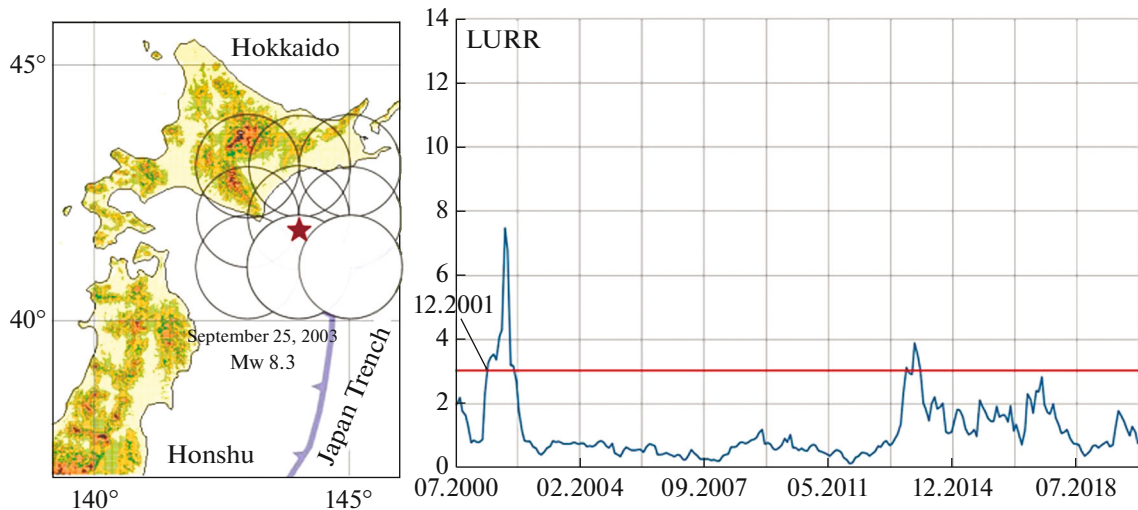


Fig. 2. Nine computational circular domains with selection of two domains in which forerunners are marked (a); graph of behavior of LURR parameter from 2000 to 2020 for epicentral zone of Tokachi-Oki earthquake (b).

variation in the nine regions over the period from 2000 to 2020. The scan mode in the retrospective analysis implies a hypothetical ability to make real-time predictions. Here, the areas are not correlated with the epicenter of the earthquake being tested. Three anomalies exceed the threshold. The anomalies have threshold crossing points: in June 2002 (Fig. 3b), in December 2001 (Fig. 3c), and in July 2017 (Fig. 3h). Two pulselike exceedances (exceedance at a single point at a step of 30 days) in the area shown in Figs. 3c and 3e cannot be considered anomalies according to our previously established rules (for a specific step). No anomalies were recorded in the other six domains. Additionally, the second, not the first, points of threshold exceedance are indicated. This was done taking into account that it is necessary to identify a possible pulse anomaly, as well as to accurately determine the real anomaly. For this purpose, one more point is required.

According to the previously adopted methodology, anomalies that are observed under the scan mode in neighboring areas and registered in time with a difference of no more than 6 months (half of the smoothing window) form a single alarm area with a waiting time of up to two years [8]. Thus, we can conclude that the calculated circular domains with centers 41° N, 144° E and 41° N, 145° E are the predicted zone for the earthquake in the period from December 2001 to December 2003. This zone fully corresponds to the spatial and temporal characteristics of the Tokachi-Oki earthquake. The first anomaly appeared in the east (145° E). Then, the area finally formed, capturing the calculated domain to the west (144° E).

Apart from the Tokachi-Oki earthquake, many other earthquakes occurred over the last 20 years. In such studies, a boundary is usually set on the magnitude of the target earthquakes. For this, in the calcula-

tion zone, including all nine calculation circular domains, the catalog was declustered following the method described in [26]. The result of declustering showed that magnitudes below six are unsuitable to be considered as target magnitudes in mid-term assessments. For example, there are 87 earthquakes left in the range $M_w = 5.0$ – 6.0 , and this number is too high to apply the LURR method. There are only three earthquakes with magnitudes $M_w > 7.0$: (September 26, 2003 ($M_w = 8.3$; 41.778° N, 144.079° E); January 29, 2004, $M_w = 7.1$ (42.946° N, 145.275° E); September 11, 2008, $M_w = 7.1$, (41.776° N, 144.152° E).

There is no evidence that the 2004 earthquake is not an aftershock of the Tokachi-Oki earthquake, especially since its magnitude indicates that it is probably a continuation of the earthquake rupture caused by the main shock in the western direction, where the fault zones closest to the epicenter extend. Moreover, it occurred a year later, which also testifies in favor of mutual dependence. In fact, out of the three listed strong earthquakes, only the 2008 earthquake remains. No precursor to this earthquake was found. Thus, when setting the lower threshold of earthquake forecasting with $M_w = 7.0$, we get a good result with one false alarm (July 2017; 43° N, 144° E), one missed target (September 2008), and one successful retrospective forecast for the Tokachi-Oki earthquake on September 25, 2003. This is a good result for a 20-year time interval with an estimated realization time of about two years.

Processing of the catalog of earthquake focal mechanisms in accordance with the MCA algorithm allowed us to compile maps of the orientation of the principal stress axes of the stress tensor (Figs. 4, 5, 8a, 8b), as well as to divide the crust by type of stress tensor

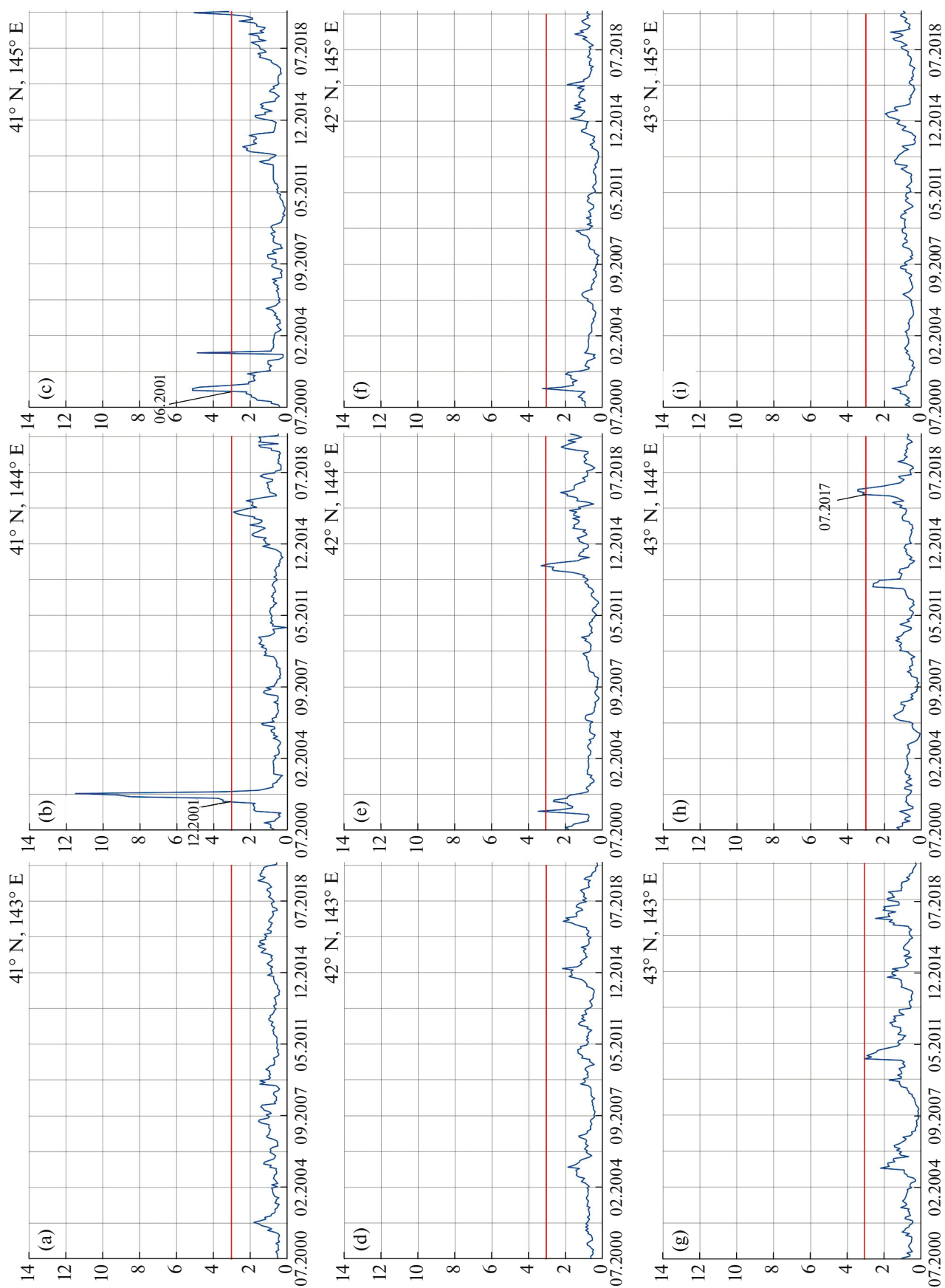


Fig. 3. Results for all computational domains. Discrimination threshold for highlighting anomalies is shown by red line.

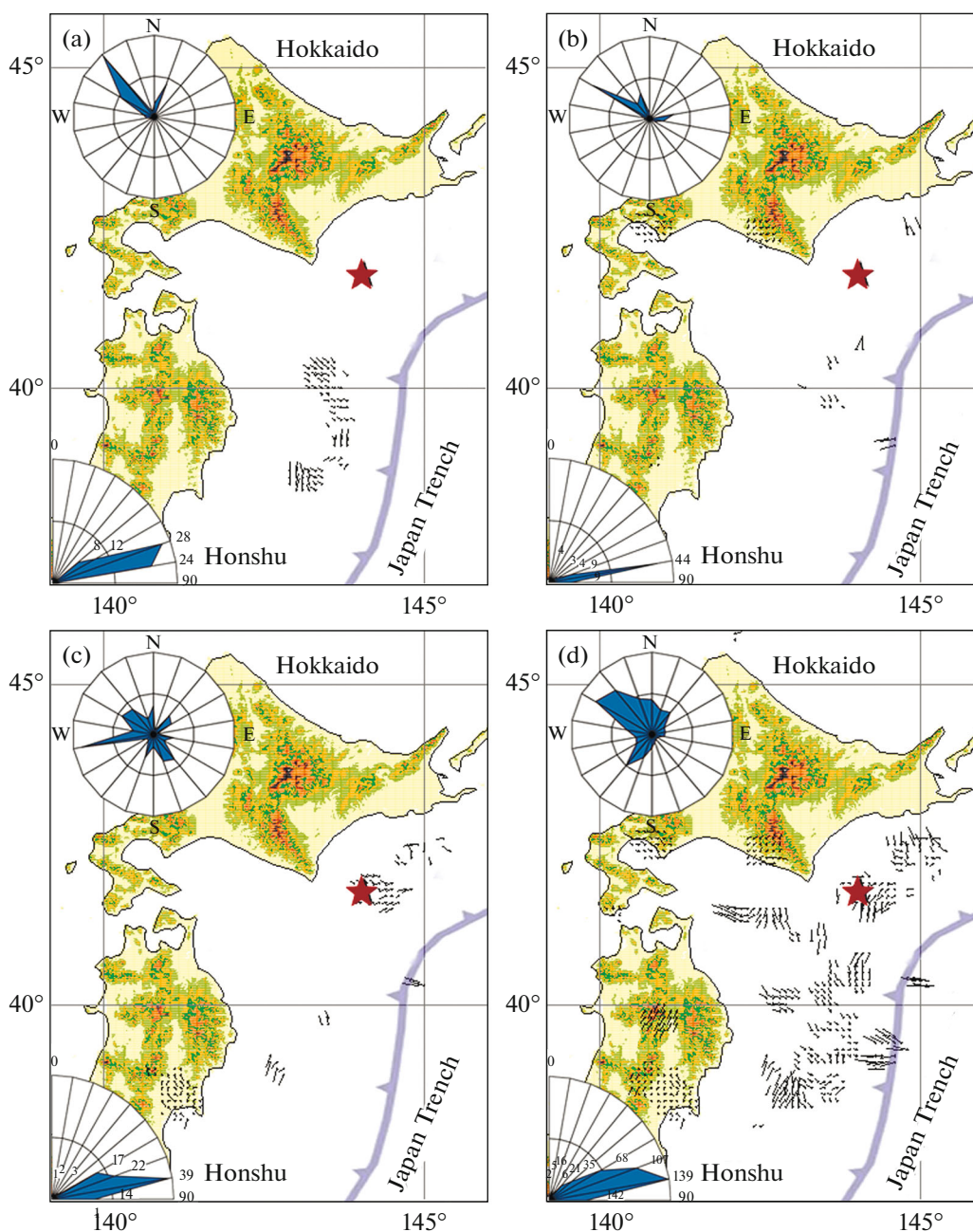


Fig. 4. Orientation of projections of plunging principal stress axes σ_1 on horizontal plane before Tokachi-Oki earthquake on September 25(26), 2003. (a) 1997–1999; (b) 2000–2001; (c) 2002–2003; (d) 1997–2003.

(ellipsoid) (Figs. 6, 8d) and the geodynamic regime (Figs. 7, 8c) determined by the type of stress state.

Figures 4, 5, 8a, and 8b show projections of the principal stress axes on the horizontal plane σ_1 (Figs. 4, 8a) and σ_3 (Figs. 5, 8b), before and after the Tokachi-Oki earthquake on September 25(26), 2003 over different time intervals (four time intervals before the earthquake—1997–1999; 2000–2001; 2002–September 25, 2003; January 1, 1997–September 25, 2003; aftershock period—September 25, 2003–Sep-

tember 25, 2004 (Figs. 8a, 8b). The orientations of the principal stress axes of the stress tensor in the crust of the Japan island arc experience a number of changes (Figs. 4, 5). Two types of stress state are combined here: those characteristic of subduction zones of the oceanic crust and those characteristic of the continental crust. Near the Japan Trench axis, the projections of the axes of maximum deviatoric extension σ_1 and compression σ_3 are oriented almost orthogonally to its strike, dipping, respectively, beneath the continental

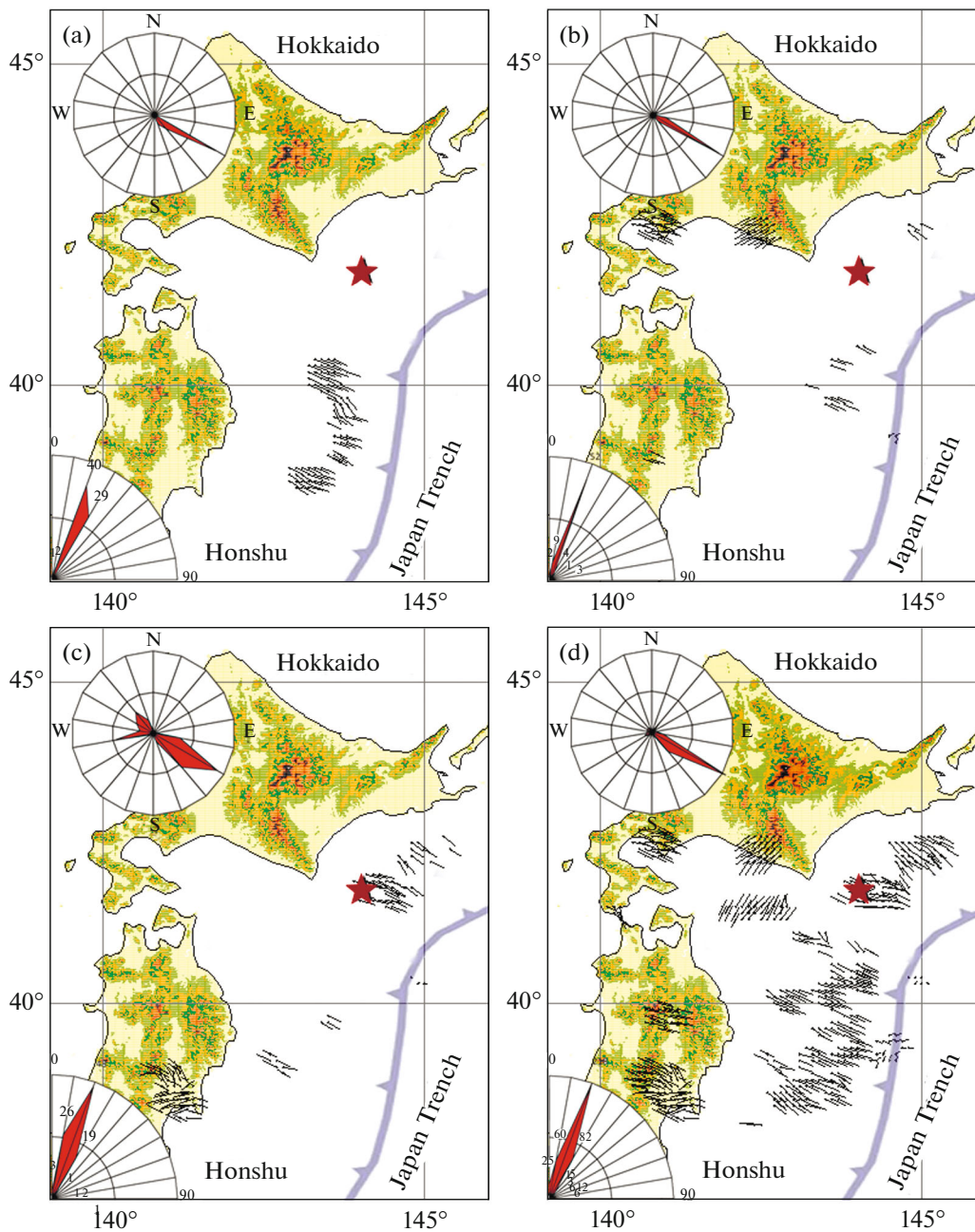


Fig. 5. Orientation of projections of plunging principal stress axes σ_3 on horizontal plane before Tokachi-Oki earthquake on September 25(26), 2003. (a) 1997–1999; (b) 2000–2001; (c) 2002–2003; (d) 1997–2003.

(extension axes) and oceanic (compression axes) plates.

In the majority of the study area, gentle dipping of the σ_3 axes is observed, while the axes of maximum deviatoric extension σ_1 have a steeper dip with a wide variation of the dip angle. The intermediate principal stress axis σ_2 is oriented along the strike of the Japan Trench. This orientation of the principal stress axes is characteristic of subduction regions and determines

the underthrust tangential stresses acting at the lithospheric basement as active forces.

The only exceptions are local areas located near Hokkaido and Honshu, where the orientation of the principal stress has significant deviations.

Type of Geodynamic Regime and Type of Stress Tensor

Based on the analysis of data on the orientation of the principal stress axes, the geodynamic zoning of the studied region by the type of stress field (geodynamic

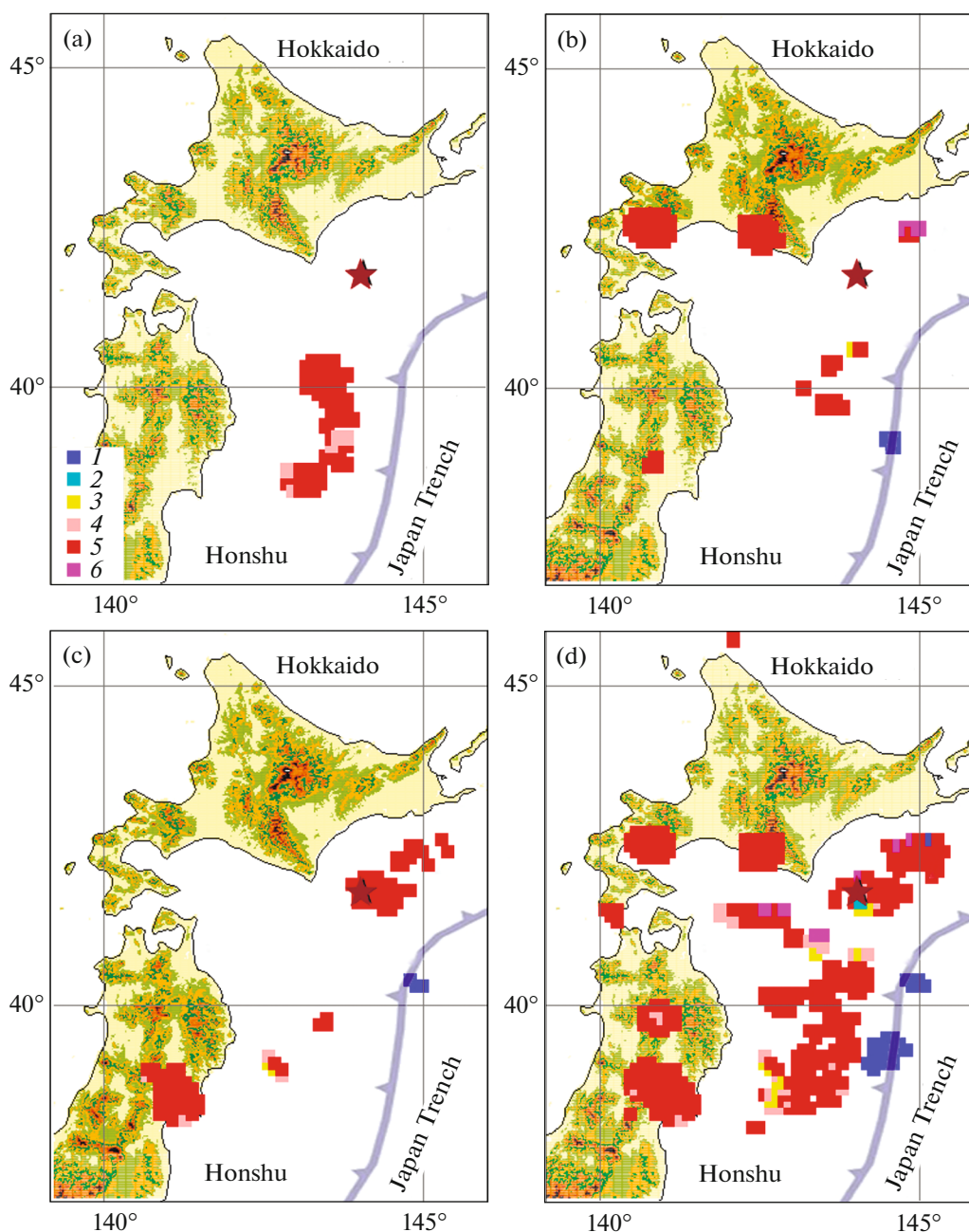


Fig. 6. Type of stress state (geodynamic regime) before the Tokachi-Oki earthquake on September 25(26), 2003. (1) extension, (2) extension-shear, (3) shear, (4) compression-shear, (5) compression, (6) oblique; (a) 1997–1999; (b) 2000–2001; (c) 2002–2003; (d) 1997–2003.

regime), which eventually determines the character of movement along the existing fault system, is presented. To determine the type of stress state, we used a scheme of division into six geodynamic types, obtained by analyzing the position of the zenith vector with respect to the principal stress axes [20]. The spectrum of possible states ranges from horizontal compression (σ_1 axis is subvertical) and shear (σ_2 axis is subvertical) to extension (σ_3 axis is subvertical).

The predominant geodynamic state of the studied area for all time intervals is the horizontal compression delete (Fig. 6). In the reconstructions for the periods from 1997 to September 25, 2003 (Fig. 6) and from September 25, 2003 to September 25, 2004 (Fig. 8c), the stress state is more fractional. Almost all sets of stress states occur here. In the conjunction zone of the Japan and South Kuril seismic focal zones, the horizontal compression environment changes to a horizontal shear environment combined with horizontal

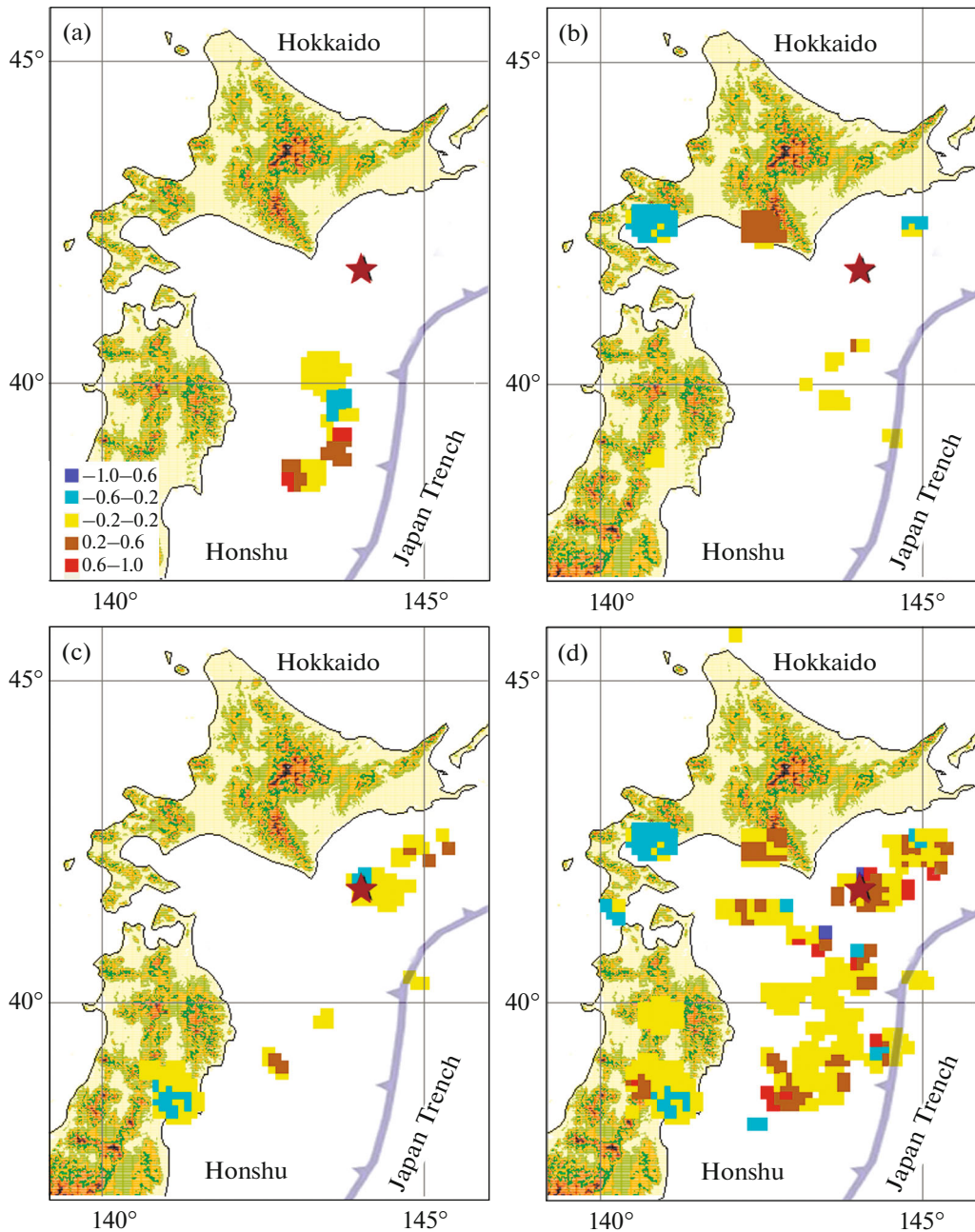


Fig. 7. Type of stress tensor—Lode—Nadai coefficient. (a) 1997–1999; (b) 2000–2001; (c) 2002–2003; (d) 1997–2003.

extension. An extensive area of extension is noted in the vicinity of the oceanic trench.

After the first step, the Lode-Nadai coefficient (Fig. 7), which determines the type of stress ellipsoid and, consequently, the type of stress tensor, is also calculated. The peak values of this parameter (+1 and -1) correspond to uniaxial compression and extension. The Lode-Nadai coefficient values, close to zero, determine the pure shear state, when the intermediate

principal deviatoric stress is zero and the other two are equal in magnitude but opposite in sign.

The main types of stress tensor of the studied area before the Tokachi-Oki earthquake are pure shear (near the axis of the Japan Trench) and its combinations with uniaxial compression (near Hokkaido) (Fig. 7). At the same time, regions with stressed areas close to uniaxial extension were noted in the crust of Hokkaido and Honshu. However, after the earthquake, estimations corresponding to the tensor near

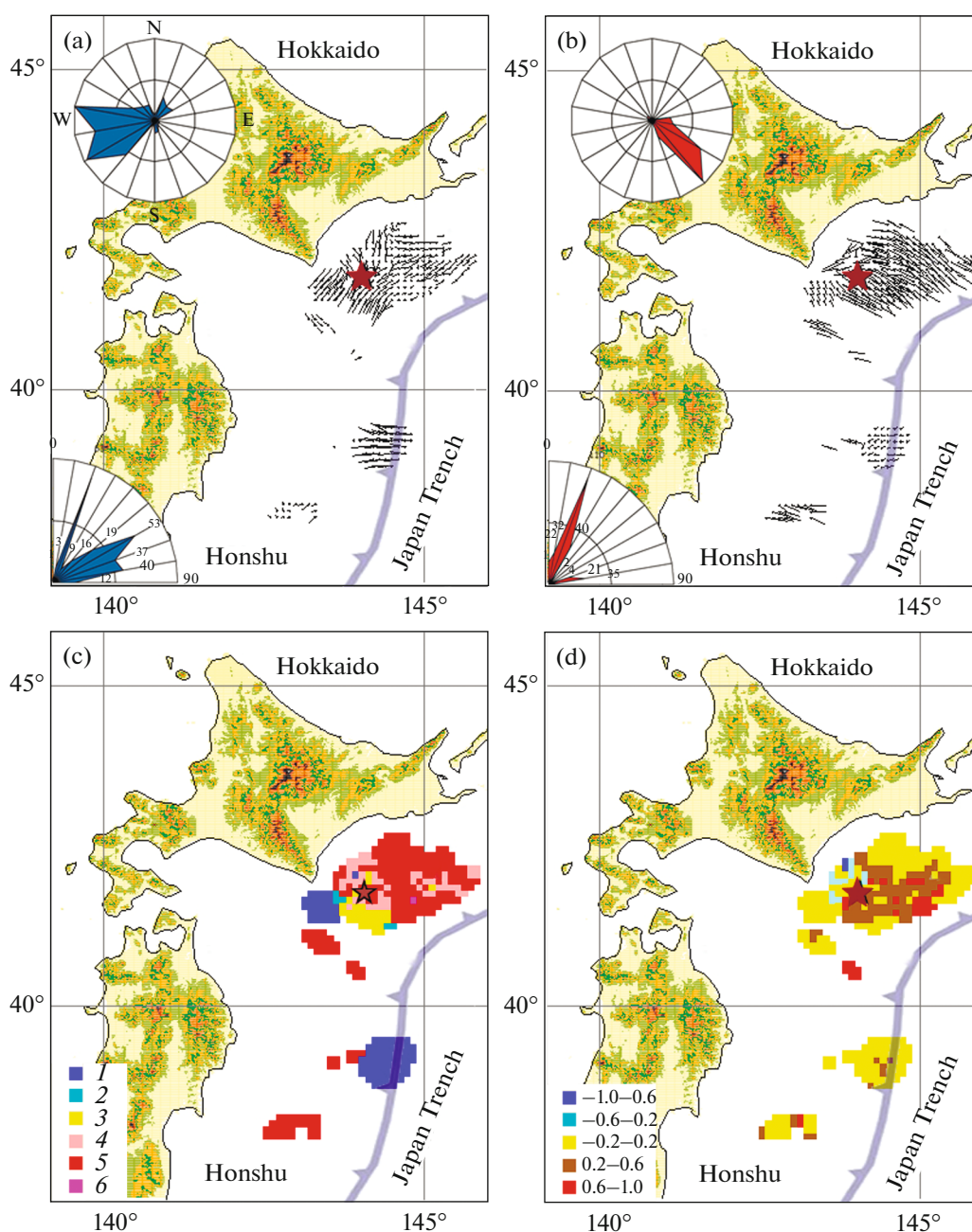


Fig. 8. Reconstruction of stress state in aftershock period. Orientation of projections of plunging principal stress axes σ_1 (a) and σ_3 (b) on horizontal plane. Type of stress state (c): (1) extension, (2) extension-shear, (3) shear, (4) compression-shear, (5) compression, (6) oblique. Type of stress tensor—Lode–Nadai coefficient (d).

uniaxial compression appeared in a sufficiently large number of reconstructed domains (Fig. 8d).

DISCUSSION

According to the MCA data, active interaction was observed on both fronts from the Hidaka zone in the period from 1997 to 2003 (before the Tokachi-Oki earthquake). From the south, the Hidaka block structures are subjected to intense arc compression from

the Amur and Pacific plates; from the north, the Okhotsk and Pacific plates actively interact at the boundary with the Hidaka zone. As well, horizontal extension areas are observed in the southeast in the zone of the Kuril–Kamchatka Deep Trench junction with the Japan Trench and further south along the Japan Trench.

Fault movements in deep trenches can occur due to various geologic and geodynamic processes. Deep trenches are adjacent to the margins of lithospheric

plates and are located at the junction of different structural blocks. The marginal fault zones may occur here. The accumulation of stresses in the fault zone can lead to subsurface shear and ground movement, which in turn can cause the formation of fault movements, especially in areas with unstable ground conditions.

Under this type of interaction in the Hidaka zone, which includes mechanically weakened blocks, the scenario of the development of a strong seismic event and movements along the belt with a predominant position of shear mechanisms are likely to occur. This is also indicated by the fact that the rupture of the strong Tokachi-Oki earthquake was localized at the boundary between the Hidaka mountains and Tokachi plain, in the contact zone between media with different rheological properties. This is confirmed by the study results [12], which show the zoning of the distribution of anisotropic properties of the medium along the eastern part of Hokkaido Island and with depth. This indicates the difference in the pattern of deformation of the medium.

The areas above the Tokachi and Kushiro plains are characterized by rather stable behavior of wave parameters in time and low anisotropy coefficients. The reason for this may be the situation when the strengthening of mechanical properties of the medium occurred under the plains. Shear deformations (discontinuous slippage) develop and accumulate in the downward plane according to the thrust (Tokachi) and normal fault (Kushiro) kinematics. These ideas are confirmed by MCA results in the aftershock period. These results show that to the north of the Hidaka zone an intensive process of destruction was realized in compression zones; to the south a small zone of compression in the contact zone of Hidaka with the Amur lithosphere plate is distinguished. However, in the Hidaka belt itself there is a zone in the northwestern direction where the destruction is characterized by shear and extension zones.

The Tokachi-Oki earthquake induced fault movements, which could have been the result of various factors related to both the earthquake itself and geologic conditions. One of the main factors was intense seismic activity induced by the Tokachi-Oki earthquake. The latter, with a moment magnitude of 8.3, resulted in significant subsurface displacements and faults in the crust, the disruption of structures and ground layers, and triggering of fault movements. Another factor is the character of the ground and geologic conditions. If the ground has an unstable texture or contains a large number of ruptures and cracks, it may be susceptible to displacements and rockfalls due to seismic forces, especially during an intense earthquake. All of these factors combined to create the conditions for ground shaking after the 2003 Tokachi-Oki earthquake.

It is interesting that the LURR anomaly, first identified in June 2001 in the computational domain centered at 41° N, 145° E, is actually located in the place where the Hidaka zone wedges into the Pacific Plate. Moreover, based on the distribution of seismic events in the study region, the western part of the calculation circular domain probably influenced the results.

In fact, the calculation circular domain centered at 41° N, 144° E, in which the anomaly is fixed after 6 months, takes up the anomaly from the neighboring area. It is possible mathematically, as 6 months is half of the sliding window. It is probable that this circular domain is strengthened by the earthquake calculations in its northwestern part also along the Hidaka mountain belt. This idea is impossible to verify. Seismic activity before the Tokachi-Oki earthquake along the belt was low-level and there was lack of data for CAM reconstruction, but the emerging instability of the zone was reflected in the LURR anomalies.

The results of this study show the LURR method in a new light and reveals the peculiarities of the “sensitivity” of this method to zones with different deformation conditions. At the same time, our results only confirm the previously announced schemes. Thus, in [23] the theoretical issues of influence of tidal forces on the triggering of earthquakes within the framework of the LURR approach are considered. It is shown that the increase in Coulomb stress arising from this phenomenon is not characteristic of all stress state regimes operating in the studied region.

Earth tides have a selective effect on faults, and this selectivity depends on their kinematic type of a rupture. The different phases of Earth tides may be loading and unloading phases under different types of stress state (horizontal compression, horizontal extension or horizontal shear). The possibility of the manifestation of trigger effects depends on the kinematic type of seismogenic faults, i.e., the geodynamic type of the present-day stress state. In addition to the direct influence of land tides on deformations in the solid earth, island arcs and coastal crustal areas are also characterized by an indirect factor in the form of additional pressure caused by sea tides. For the ocean floor, it is an additional vertical pressure; for the island arc and shelf crust—a lateral pressure. Indirect factors significantly complicate the effect of the impact of land tides on the Earth's crust, in some cases completely levelling out the influence of the direct factor.

The normal faults and strike-slip faults are significantly more dangerous for the realization of the trigger effect of land tides. During the realization of these tectonic motions, they are possible to approach the limit state at the moments of their being in the phase of uplift. The realization of the trigger effect for reverse and strike-slip faults at the trough phase is less probable. Anyway, it can be possible because of the significantly smaller increment of Coulomb stresses. It is important to note here that strike-slip faults that can

be activated by land tides at the phase of uplifting or at the phase of subsidence, at the phases of subsidence or uplifting, respectively, are characterized by a decrease in Coulomb stresses.

Since the maximum extension is manifested in the submeridional direction, the greatest impact will be during development of the sublatitudinal normal fault. Accordingly, additional compression stress in the subsidence region occurs submeridionally and sublatitudinally, resulting in a greater probability of activation of overthrust faults. Thus, faults in seismogenic zones of the Earth's crust are constantly in a precritical state and respond differently to loading and unloading. The occurrence of a strong earthquake dissipates part of the accumulated elastic energy and removes the fault from the critical state. Subsequently, tectonic loading returns the fault back to the critical state.

CONCLUSIONS

The present paper proposes an original approach to the LURR method, which was applied to analyze seismicity of Hokkaido. To process the data, we used the Seis-ASZ program complex developed at the Institute of Marine Geology and Geophysics FEB RAS (Yuzhno-Sakhalinsk) and the authors' methods for determining the processing parameters and computational samples. In particular, it concerns the definition of parameters for calculating the LURR parameter in time, the rules for detecting LURR anomalies, the conditions for scanning an area that is many times larger than the calculated area, and the selection of forecast objects. The study was carried out using seismic data from the part of Hokkaido where one of the recent strongest earthquakes in the world occurred: the Tokachi-Oki earthquake (September 25, 2003, $M_w = 8.3$).

The calculations showed satisfactory results in detecting LURR anomalies before strong earthquakes. The active seismicity of Hokkaido island is definitely characterized by suppression of anomalies before moderate earthquakes, which generally improved the result. In case of a large number of earthquakes in the sample, the moving-average filter always suppresses perturbations. In particular, the presence of variations before events with $M_w = 6.0$ or $M_w = 7.0$ can be considered a perturbation for anomaly detection before strong earthquakes. In the calculations, there are no evident anomalies in the determination of a precursor before the Tokachi-Oki earthquake. As a result, with a minimum level of false alarms (one), we obtained one retrospective forecast for the 20-year period, which by all characteristics fits only the strongest earthquake from the sample, i.e., the Tokachi-Oki earthquake. For the first time in our practice, the results of LURR analysis were compared with the results of MCA reconstruction. The main task was to show the dynamics of the earthquake preparation process in its

final part: from the appearance of the LURR anomaly to the earthquake. The period before the appearance of the anomaly (a time interval of about 5 years) was also taken into consideration. The results met expectations. Despite the small periods (1997–1999; 2000–2001; 2002–2003; 1997–2003; 2003–2004) the MCA revealed the characteristic stages of instability development in the area of the Hidaka tectonic belt, which completely agrees with the geological and tectonic ideas about this territory. Moreover, the LURR anomalies, which appeared at the final stage (when the main areas of compression along the belt were worked out), determine the structures of the Hidaka tectonic belt as a zone of the future catastrophe, from the place of belt wedging into the Pacific Plate with the earthquake forerunner moving in time to the northwest along the belt. In the future, it is of interest to develop the combination of the two methods (LURR and MCA).

FUNDING

This work was supported by ongoing institutional funding. No additional grants to carry out or direct this particular research were obtained.

CONFLICT OF INTEREST

The authors of this work declare that they have no conflicts of interest.

REFERENCES

1. V. A. Aprodov, *Nature of the World. Earthquake Zones* (Mysl', Moscow, 2000).
2. Yu. G. Gatinsky and D. V. Rundkvist, "Geodynamics of Eurasia: Plate Tectonics and Block Tectonics," *Geotectonics* **38** (1), 1–16 (2004).
3. V. M. Grannik, *Extended Abstract of Doctoral Dissertation in Geology and Mineralogy* (Vladivostok, 2006).
4. A. S. Zakupin, "Software for analysis of instability of seismic process," *Geoinformatika*, No. **1**, 34–43 (2016).
5. A. S. Zakupin, Yu. N. Levin, N. V. Boginskaya, and O. A. Zherdeva, "Development of medium-term prediction methods: a case study of the August 14, 2016 Onor ($M_w = 5.8$) earthquake on Sakhalin," *Russ. Geol. Geophys.* **59** (11), 1526–1532 (2018). <https://doi.org/10.1016/j.rgg.2018.10.012>
6. A. S. Zakupin and N. V. Boginskaya, "Mid-term assessments of seismic hazards on Sakhalin Island using the LURR method: new results," *Geosyst. Transition Zones* **4** (2), 169–177 (2020). <https://doi.org/10.30730/gtrz.2020.4.2.160-168.169-177>
7. A. S. Zakupin, L. M. Bogomolov, and N. V. Boginskaya, "Successive application of methods of analysis of seismic sequences LURR and SRP for earthquake prediction on Sakhalin," *Geofiz. Protsessy Biosfera*, No. **1**, 66–78 (2020).

8. A. S. Zakupin and N. V. Boginskaya, "Mid-term earthquake prediction using the LURR method on Sakhalin Island: A summary of retrospective studies for 1997–2019 and new approaches," *Geosyst. Transition Zones* **5** (1), 27–45 (2021).
<https://doi.org/10.30730/gtr.2021.5.1.027-045>
9. *Fault Map of the USSR and Neighboring Countries. 1:2,500,000*, Ed. by A. V. Sidorenko (Mingeo–AN SSSR, Moscow, 1980).
10. A. I. Kozhurin, T. K. Pinegina, V. V. Ponomareva, E. A. Zelenin, and P. G. Mikhailyukova, "Rate of collisional deformation in Kamchatsky Peninsula, Kamchatka," *Geotectonics* **48** (2), 122–138 (2014).
<https://doi.org/10.1134/s001685211402006x>
11. G. G. Kocharyan and I. V. Batukhtin, "Laboratory studies of slip along faults as a physical basis for a new approach to short-term earthquake prediction," *Geodynam. Tectonophys.* **9** (3), 671–691 (2018).
<https://doi.org/10.5800/gt-2018-9-3-0367>
12. M. N. Luneva, "Seismic anisotropy and spatial distribution of local earthquake splitting parameters along the eastern part of Hokkaido Island," *Fiz. Mezomekhan.* **11** (1), 37–43 (2008).
13. P. V. Makarov, "Mathematical theory of evolution of loaded solids and media," *Fiz. Mezomekhan.* **11** (3), 19–35 (2008).
14. V. A. Nikolaev, "Spatial and temporal peculiarities of connection of strong earthquakes with tidal phases," in *Induced seismicity* (Nauka, Moscow, 1994), pp. 103–114.
<https://doi.org/10.22449/2413-5577-2019-2-48-58>
15. V. A. Nikolaev, "Response of strong earthquakes to phases of earth tides," *Fiz. Zemli*, No. **11**, 49–58 (1994).
16. L. N. Poplavskaya, A. O. Bobkov, A. N. Boichuk, N. A. Mitaleva, L. S. Oskorbin, M. I. Rudik, M. I. Strel'tsov, I. N. Tikhonov, and A. I. Malyshev, *Shimushir Earthquake on January 9, 1989* (IMGiG DVO RAN, Yuzhno-Sakhalinsk, 1991).
17. T. G. Rautian, "Earthquake energy," in *Methods of Detailed Study of Seismicity* (Elsevier BV, 1960), pp. 75–114.
[https://doi.org/10.1016/0160-9327\(60\)90032-6](https://doi.org/10.1016/0160-9327(60)90032-6)
18. Yu. L. Rebetskii, "Development of the method of cataclastic analysis of shear fractures for tectonic stress estimation," *Dokl. Earth Sci.* **388** (1), 72–76 (2003).
19. R. L. Yu, L. A. Sim, O. V. Lunina, and I. A. Dzyuba, "Application of the method of cataclastic analysis of spalling to paleo-stress reconstruction," in *Proceedings of the Tectonic Meeting* (Novosibirsk, 2004), pp. 103–106.
20. Yu. L. Rebetskii, *Tectonic Stresses and Strength of Rock Massifs* (Nauka, Moscow, 2007).
21. Yu. L. Rebetskii, O. A. Kuchai, and A. V. Marinin, "Stress and deformation of the Earth's crust in the Altai–Sayan mountainous area," *Russ. Geol. Geophys.* **54** (2), 206–222 (2013).
22. Yu. L. Rebetskii, "Stress state of Japan's lithosphere before the catastrophic Tohoku earthquake on March 11, 2011," *Geodyn. Tectonophys.* **5** (3), 469–506 (2014).
23. Yu. L. Rebetskii, "Concerning the theory of LURR based deterministic earthquake prediction," *Geosyst. Transition Zones* **5** (3), 192–208 (2021).
<https://doi.org/10.30730/gtr.2021.5.3.192-208.208-222>
24. L. A. Savostin, A. I. Verzhbitskaya, and B. V. Baranov, "Modern tectonics of the Okhotsk region," *Dokl. Akad. Nauk SSSR* **266** (4), 961–965 (1982).
25. L. A. Sim, L. M. Bogomolov, G. V. Bryantseva, and P. A. Savichev, "Patterns of transition zone between Eurasian and North American plates (by example of stressed state of the Sakhalin Island)," *Geosyst. Transition Zones* **1** (1), 3–22 (2017).
<https://doi.org/10.5800/gt-2017-8-1-0237>
26. V. B. Smirnov, "Experience in assessing the representativeness of earthquake catalog data," *Vulkanol. Seismol.*, No. 4, 93–105 (1997).
27. O. E. Starovoi, R. S. Mikhailova, E. A. Rogozhin, and L. S. Chepkunas, "Northern Eurasia," *Zemletryaseniya Sev. Evrazii* **12**, 11–28 (2009).
28. E. N. Erlikh, *Modern Structure and Quaternary Volcanism of the Western Pacific Rim* (Nauka, Sibirskoe otdelenie, 1979).
<https://doi.org/10.1086/ahr/76.1.174>
29. J. Berger, W. Farrell, J. C. Harrison, J. Levine, and D. C. Agnew, *ERTID 1: A Program for Calculation of Solid Earth Tides* (Scripps Institution of Oceanography, 1987).
30. M. E. Chapman and S. C. Solomon, "North American-Eurasian Plate Boundary in northeast Asia," *J. Geophys. Res.* **81** (5), 921–930 (1976).
<https://doi.org/10.1029/jb081i005p00921>
31. R. A. Harris, "Introduction to special section: stress triggers, stress shadows, and implications for seismic hazard," *J. Geophys. Res.: Solid Earth* **103** (B10), 24347–24358 (1998).
<https://doi.org/10.1029/98jb01576>
32. A. Ismail-Zadeh, S. Honda, and I. Tsepelev, "Linking mantle upwelling with the lithosphere descent and the Japan Sea evolution: a hypothesis," *Sci. Rep.* **3** (1), 1137 (2013).
<https://doi.org/10.1038/srep01137>
33. N. Kato, H. Sato, M. Orito, K. Hirakawa, Ya. Ikeda, and T. Ito, "Has the plate boundary shifted from central Hokkaido to the eastern part of the Sea of Japan?," *Tectonophysics* **388** (1–4), 75–84 (2004).
<https://doi.org/10.1016/j.tecto.2004.04.030>
34. V. Keilis-Borok, P. Shebalin, A. Gabrielov, and D. Turcotte, "Reverse tracing of short-term earthquake precursors," *Phys. Earth Planet. Inter.* **145** (1–4), 75–85 (2004).
<https://doi.org/10.1016/j.pepi.2004.02.010>
35. G. Kimura, S. Miyashita, and S. Miyasaka, "Collision Tectonics in Hokkaido and Sakhalin," in *Accretion Tectonics in the Circum-Pacific Regions*, Ed. by M. Hashimoto and S. Uyeda (Terrapub, Tokyo, 1983), pp. 123–134.
https://doi.org/10.1007/978-94-009-7102-8_9
36. W. Sun, "Initiation of subduction of a plate," *Earth Monit.* **5** (4), 510–514 (1983).
<https://doi.org/10.1016/j.sesci.2017.10.001>
37. J. Lemaitre, "Formulation and identification of damage kinetic constitutive equations," in *Continuum Dam-*

- age Mechanics Theory and Application*, Ed. by D. Krajcinovic (Springer Vienna, Wien, 1987), pp. 37–89. https://doi.org/10.1007/978-3-7091-2806-0_2
38. K. Mogi, “Deep seismic activities preceding the three large ‘shallow’ earthquakes off south-east Hokkaido, Japan—the 2003 Tokachi-oki earthquake, the 1993 Kushiro-oki earthquake and the 1952 Tokachi-oki earthquake,” *Earth, Planets Space* **56** (3), 353–357 (2004). <https://doi.org/10.1186/bf03353064>
 39. K. A. Murase, “A Characteristic Change in Fractal Dimension Prior to the 2003 Tokachi-oki Earthquake (MJ = 8.0), Hokkaido, Northern Japan,” *Earth, Planets Space* **56** (3), 401–405 (2003). <https://doi.org/10.1186/bf03353072>
 40. K. Nakamura, “Possibility of a nascent plate boundary at the eastern margin of the Japan Sea,” *Bull. Earthq. Res. Inst. Univ. Tokyo* **58** (12), 711–722 (1983). [https://doi.org/10.1016/0198-0254\(85\)93658-1](https://doi.org/10.1016/0198-0254(85)93658-1)
 41. K. Mogi, “Preliminary observations on the Tokachi-Oki, Japan, Earthquake of Sept. 26, 2003,” *EERI Newslett* **37** (12), 1–4 (2003). <https://doi.org/10.1186/bf03353064>
 42. Yu. L. Rebetsky, N. A. Sycheva, O. A. Kuchay, and R. E. Tatevossian, “Development of inversion methods on fault slip data. Stress state in orogenes of the central Asia,” *Tectonophysics* **581**, 114–131 (2012).
 43. T. Seno, “New plate boundary around Japan and its change after 0.5 Ma,” *Kagaku (Sci.)* **57**, 84–93 (1987). <https://doi.org/10.3998/mpub.11422327.cmp.24>
 44. T. Seno, T. Sakurai, and S. Stein, “Can the Okhotsk Plate be discriminated from the North American plate?,” *J. Geophys. Res.: Solid Earth* **101** (B5), 11305–11315 (1996). <https://doi.org/10.1029/96jb00532>
 45. P. Shebalin, V. Keilis-Borok, I. Zaliapin, S. Uyeda, T. Nagao, and N. Tsybin, “Advance short-term prediction of the large Tokachi-oki earthquake, September 25, 2003, M = 8.1 A case history,” *Earth, Planets Space* **56** (8), 715–724 (2004). <https://doi.org/10.1186/bf03353080>
 46. H. Shiobara and H. Shimizu, “Success in direct observation of off-Tokachi earthquake: JAMSTEC,” *S T Today* **15** (12), 6 (2003).
 47. G. A. Sobolev, “Series of asymmetric pulses in the low-frequency range (Periods of 1–300 min) of microseisms as indicators of a metastable state in seismically active zones,” *Izv., Phys. Solid Earth* **44** (4), 261–274 (2008). <https://doi.org/10.1134/s11486-008-4001-7>
 48. S. Watada, T. Kunugi, K. Hirata, H. Sugioka, K. Nishida, S. Sekiguchi, J. Oikawa, Yo. Tsuji, and H. Kanamori, “Atmospheric pressure change associated with the 2003 Tokachi-Oki earthquake,” *Geophys. Res. Lett.* **33** (24), L24306 (2006). <https://doi.org/10.1029/2006gl027967>
 49. Yo. Yamanaka and M. Kikuchi, “Source process of the recurrent Tokachi-oki earthquake on September 26, 2003, inferred from teleseismic body waves,” *Earth, Planets Space* **55** (12), e21–e24 (2003). <https://doi.org/10.1186/bf03352479>
 50. X. Yin, C. Yin, and X. Chen, “The precursor of instability for nonlinear systems and its application to earthquake prediction—the load-unload response ratio theory,” *Sci. China* **34**, 977–986 (1991). <https://doi.org/10.1029/gm083p0055>
 51. X. C. Yin, C. Yin, and X. Z. Chen, “The precursor of instability for nonlinear system and its application to earthquake prediction - The load-unload response ratio theory. Nonlinear dynamics and predictability of geophysical phenomena,” *Geophys. Monograph* **18**, 55–60 (1994).
 52. X. C. Yin, X. Z. Chen, Z. P. Song, and C. Yin, “A new approach to earthquake prediction: The Load/Unload Response Ratio (LURR) theory,” *Pure Appl. Geophys.* **145** (3-4), 701–715 (1995). <https://doi.org/10.1007/bf00879596>
 53. X. C. Yin, L. P. Zhang, H. H. Zhang, C. Yin, Y. Wang, Y. Zhang, K. Peng, H. Wang, Z. Song, H. Yu, and J. Zhuang, “LURR’s twenty years and its perspective,” *Pure Appl. Geophys* **163**, 2317–2341 (2006). <https://doi.org/10.1007/s00024-006-0135-x>
 54. I. E. Zakharenkova, I. I. Shagimuratov, A. Krankowski, and A. F. Lagovsky, “Precursory phenomena observed in the total electron content measurements before great Hokkaido earthquake of September 25, 2003 (M = 8.3),” *Stud. Geophys. Geod.* **51**, 267–278 (2003).
 55. <https://www.globalcmt.org/>
 56. <http://www.fnet.bosai.go.jp/>

Recommended for publishing by V.G. Bykov

Translated by D. Voroshchuk

Publisher’s Note. Pleiades Publishing remains neutral with regard to jurisdictional claims in published maps and institutional affiliations.